5

Characterization of Carbon from the Bark of *P. juliflora* by Conventional Heating Method

5.1. Introduction

The electrochemical performance of carbon synthesized from the stick of *P. juliflora* by conventional heating method demonstrates the low specific capacitance as discussed in the previous Chapter. As another source, the bark of *P. juliflora* has been used for synthesizing carbon through the conventional heating method. The resultant carbon sample has been subjected to XRD, Raman, FESEM-EDX, HRTEM, BET, CV, GCD and EIS analysis. The outcomes are elaborately discussed in this Chapter. Conventionally, the carbon prepared from the bark of *P. juliflora* is termed as B-Carbon throughout the discussion.

5.2. X-Ray Diffraction Analysis of B-Carbon

The XRD pattern of B-Carbon is shown in Figure 23. It is fitted by using origin software. The obtained XRD peak of B-Carbon at 24.14° indexed to (002) plane is broad when compared with the (002) peak and (001) plane at 45.28° of S-Carbon observed at 25.23° indicating graphitic carbon peaks with disordered structure. The disordered structure arises due to the randomly oriented hexagonal carbon layers that are not stacked parallel for longer range. Similar discussion on XRD peaks holds good as of S-Carbon hereto. The intensity ratio between (002) and (001) plane provides the information of crystalline nature of the sample. For B-Carbon, the intensity ratio of these two peaks is 2.75 that is lower than the S-carbon.

5.3. Raman Analysis of B-Carbon

Raman spectra of B-Carbon is given in Figure 24. The inset shows the fitted Raman spectra of S-Carbon. It shows the D and G bands at 1339 cm^{-1} and 1593 cm^{-1} due to the vibrations of A_{1g} and E_{2g} mode respectively. These bands are less prominent compared with S-Carbon attributed to higher order of disorderliness. The intensity ratio between D and G bands estimates the degree of disorder/ degree of graphitization. Figure 24, shows the less intense G band compared with D band. In the present case, I_D/I_G value is 1.09 and

the obtained value is higher than the I_D/I_G ratio of S-Carbon verifying the disorderliness of the sample. The Raman results are supported by XRD analysis of B-Carbon where disorderliness brought in broad and blunt peaks in XRD. Similar results have been observed in the reported articles of various biomass derived carbon which are mentioned in the previous Chapter.

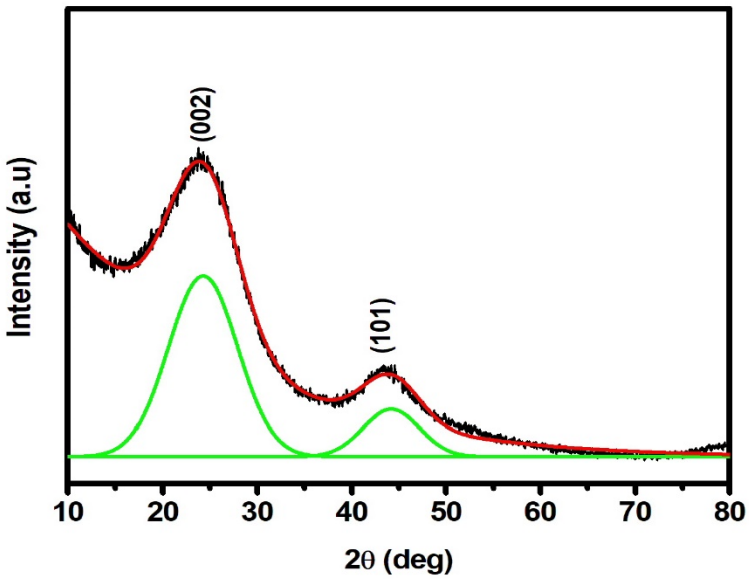

Figure 23 - X-ray Diffractogram of B-Carbon

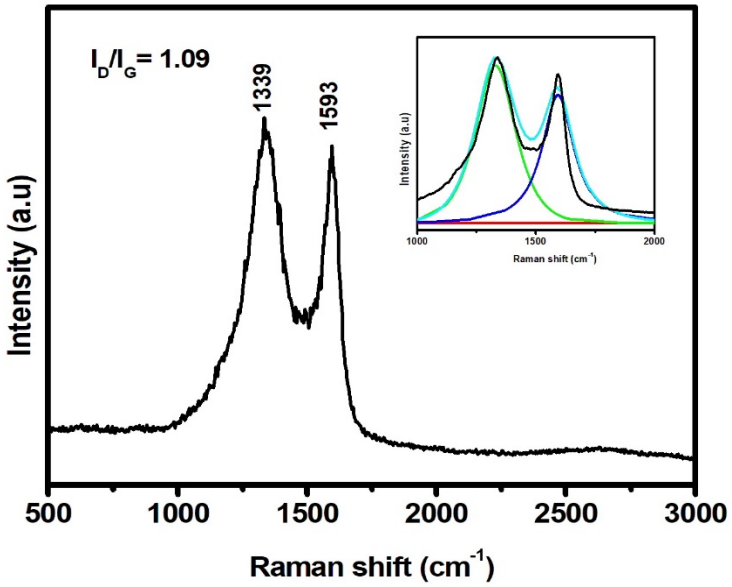

Figure 24 - Raman spectra of B-Carbon

Further peaks at 423 cm^{-1} and 2675 cm^{-1} corresponds to double resonance mechanism of D band at 1339 cm^{-1}. The peak at 2900 cm^{-1} corresponds to the weak bands of 2D+D"(**Kawashima & Katagiri, 1995; Sole et al., 2014)**. Since the influence of weak band D" is seen at 2900 cm^{-1}, the degree of disorderliness can be understood as high. The less disordered graphitic carbon does not show up influences of D" in Raman analysis.

5.4. FESEM Analysis of B-Carbon

The morphological features of B-Carbon at different magnifications are shown in Figure 25a. The morphology of the B-Carbon is entirely different from the S-Carbon which may be due to the variation in biomass precursor. It shows uniformly distributed porous morphology than the S-Carbon sample. At 2 µm scale, the pore diameter is approximately in the range of 2 µm suggesting the presence of macropores in the B-Carbon. Magnifying the sample to 100 nm scale of B-Carbon from *P. juliflora* biomass, shows well distributed and higher concentration of pores throughout the sample compared to S-Carbon. Further, it exhibits pore size in the range of~ 15nm indicating the presence of mesopores in the B-Carbon. Figure 25b shows the FFT processed micrographs show flaky structures with domains and cleavages indicating the possibility of macro and micropores in between the flaky structures. Other reports available on activated carbon from various biomass **(Elaiyappillai et al., 2019; Jain et al., 2021; Wang et al., 2016)** exhibits porous morphology in the range of 200 nm. In the reported works, carbon has been prepared from the various biomass such as Cucumis melo fruit, European deciduous tree and cabbage leaves. The steps involved in the synthesis procedures of reported activated carbon are pre-carbonization and chemical activation process. But, in this case, without pre-carbonization and post activation well developed porous morphology have been attained. In addition, compared to S-Carbon, a highly porous morphology has been observed in B-Carbon. It implies that apart from preparation procedures, the biomass precursor also plays a role to achieve porous morphology. The reported fact of low crystalline carbon materials has highly porous structure **(Ahmed et al., 2018; Mitravinda et al., 2018; Rawal et al., 2018)** and is also evident in the present work.

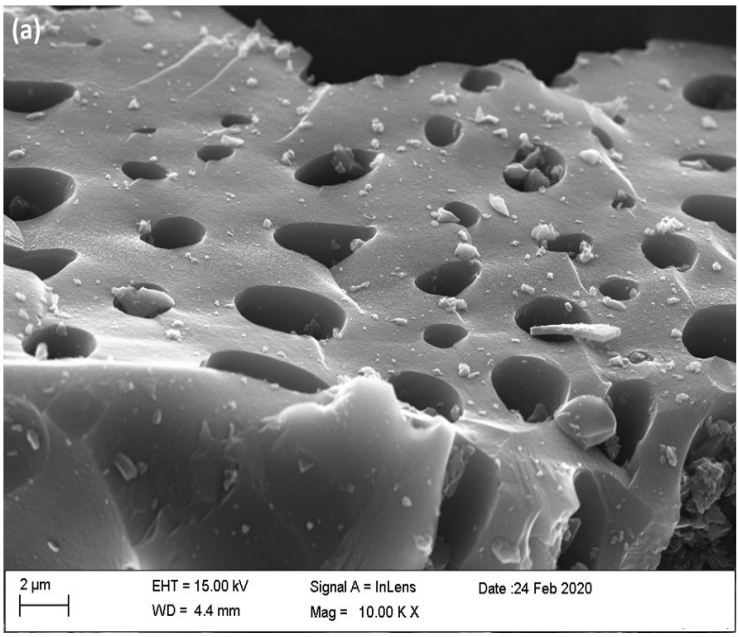

Figure 25a - FESEM micrograph of B-Carbon at lower magnification

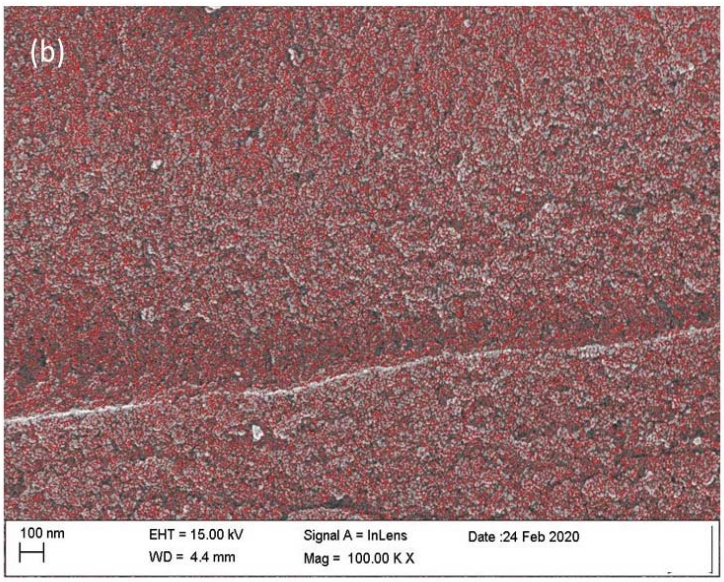

Figure 25b – FFT processed FESEM micrograph of B-Carbon at higher magnification

5.5. HR-TEM Analysis of B-Carbon

HRTEM analysis provides the structural features of B-Carbon, shown in Figure 26a and 26b. Compared with S-Carbon, highly disordered morphology is seen in the HRTEM micrograph of 10 nm scale. Apart from this, there is no vertical planes related to the

graphitic layer are seen in 10nm scale which attributes to the low crystalline nature of the sample. This is corroborated with the XRD and Raman analysis. The obtained micrographs are fast Fourier transformed after z projection processed with ImageJ for better visibility of highly disordered graphitic formation as seen in Figure 26c.

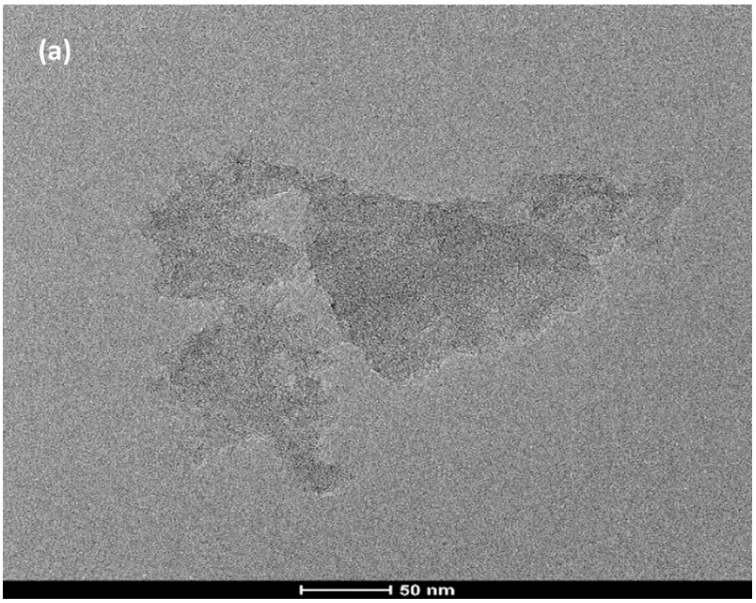

Figure 26a - HRTEM images of B-Carbon at lower magnification

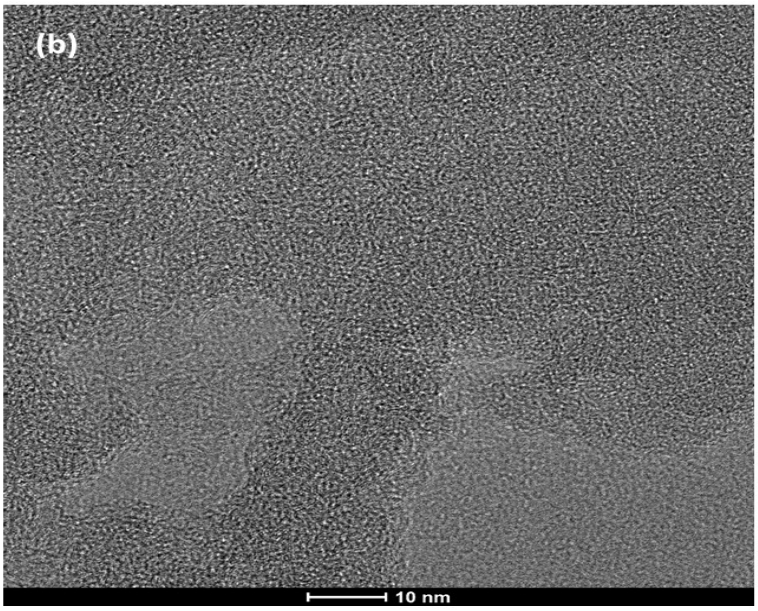

Figure 26b - HRTEM images of B-Carbon at higher magnification

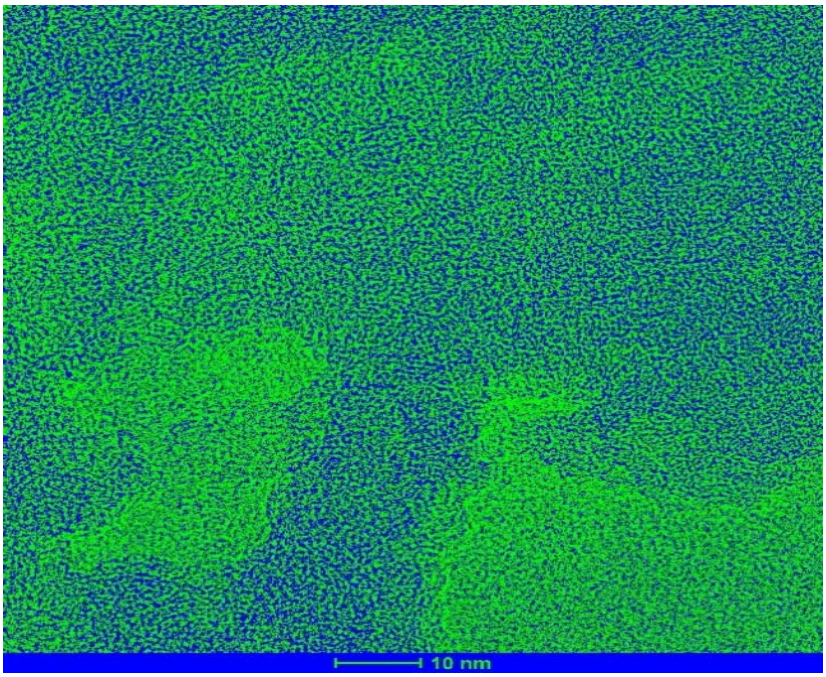

Figure 26c - FFT processed HRTEM image of B-Carbon at higher magnification

5.6. Elemental Analysis of B-Carbon

The elemental compositions of B-Carbon is shown in Figure 27. It confirms the presence of carbon, nitrogen and oxygen elements in the prepared sample. The atomic weight percentage of the elements are given in Table 12. The B-Carbon does not contain metal (Ca, Si, K) elements. Hence, B-Carbon shows highly porous morphology than S-Carbon. Notably, the atomic weight percentage of carbon in B-Carbon is 91.44%. The atomic weight of carbon present in the B-Carbon is compared with the previously reported articles of carbon derived from various biomass which are discussed in previous Chapter. In the present work, the higher atomic weight percentage of carbon has been achieved by simple preparation method. But the similar synthesis procedure has been adopted in the case of S-carbon which gives low atomic weight percentage of carbon (as explained in Chapter 4) that concludes that yield of carbon content not only depends on the preparation method as well as biomass precursor (bark of *P. juliflora*).

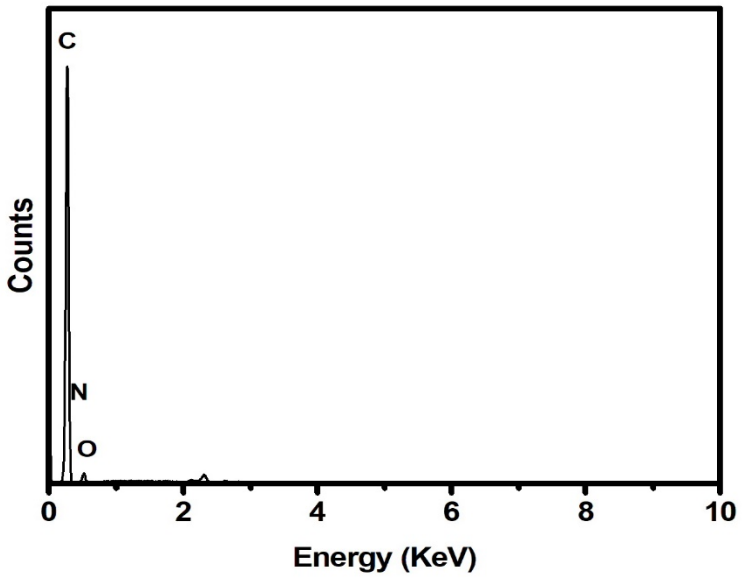

Figure 27 - EDX spectrum of B-Carbon

Table 12 - Elemental composition of B-Carbon

Elements	At. Wt.%
Carbon	**91.44**
Oxygen	6.68
Nitrogen	1.88

5.7. BET Surface Area Analysis of B-Carbon

The BET analysis of B-Carbon is given in Figure 28. At low relative pressure (P/P_0 <0.1), isotherm shows sharply increased N_2 adsorption/desorption which indicates that the B-Carbon sample has abundant micropores. In this region, the isotherms are overlapped. It implies that nitrogen uptake by B-carbon sample containing micropores is reversible. Besides, the hysteresis loop observed in the midrange ($0.4 < P/P_0 < 0.8$) implies the presence of mesopores.

In addition to micropores and mesopores, the rapid increase in N_2 adsorption at high relative (P/P_0 = 0.9 – 1.0) pressure indicates the contribution of macropores. Comparing B-carbon with S-Carbon, the former exhibits the hysteresis loop with smaller

area indicating the sample has larger concentrations of micropores than the mesopores. Smaller pores give rise to larger surface area and it can be calculated from BET analysis. The value is 703 m^2g^{-1} which is comparably higher than S-Carbon. In the case of S-Carbon, surface area is mainly contributed by the mesopores resulting in lower surface area (6.38 m^2g^{-1}). Apart from that, there is no metal contents such as K, Ca and Si in B-Carbon as seen in EDAX analysis. Hence, there is a less possibility of clogging the pores of B-Carbon resulting in high degree of micropore distribution which enhances the specific surface area of the B-Carbon. Also the clear image of strangled threads of highly disordered graphite that forming a mesh like structure, as seen from the HRTEM micrograph, will be the reason for the increase in surface area.

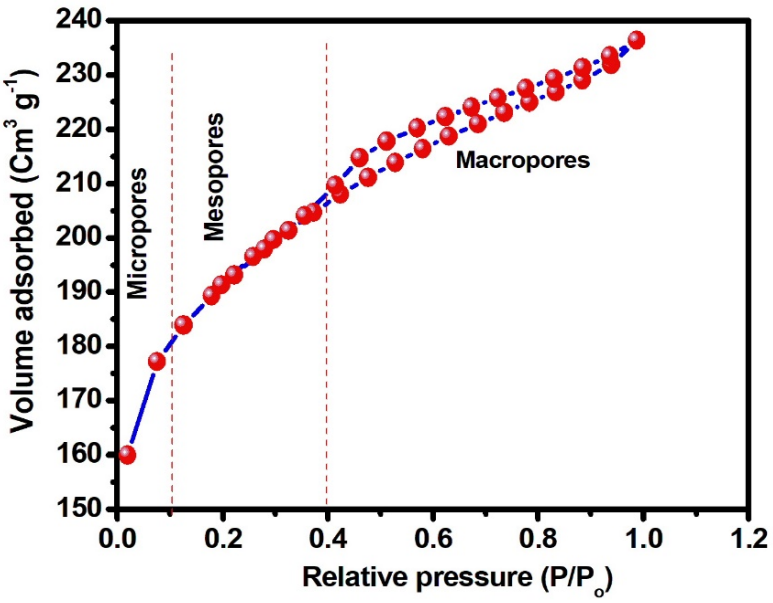

Figure 28 - BET analysis of B-Carbon

Figure 29 depicts a pore size distribution diagram. It is clear that the distribution of B-Carbon in the micropore region is higher than that of S-Carbon. In N_2 adsorption/desorption isotherms of B-Carbon, the smaller region of hysterisis loop closely corresponds to the higher distribution of micropores. The pore volume and average pore diameter of B-Carbon from the Barrett, Joyner, and Halenda (BJH) method is 0.116 cm^3g^{-1} and 2.2 nm. Further, Figure 29 reveals that the majority of pores are scattered in the range of 2 nm to 8 nm, implying that micropores and mesopores are predominant in this case. Compared with

S-Carbon, the difference in surface area and pore size distribution of B-Carbon is expected to occur the different results in electrochemical analysis. The following sections will go through this in details.

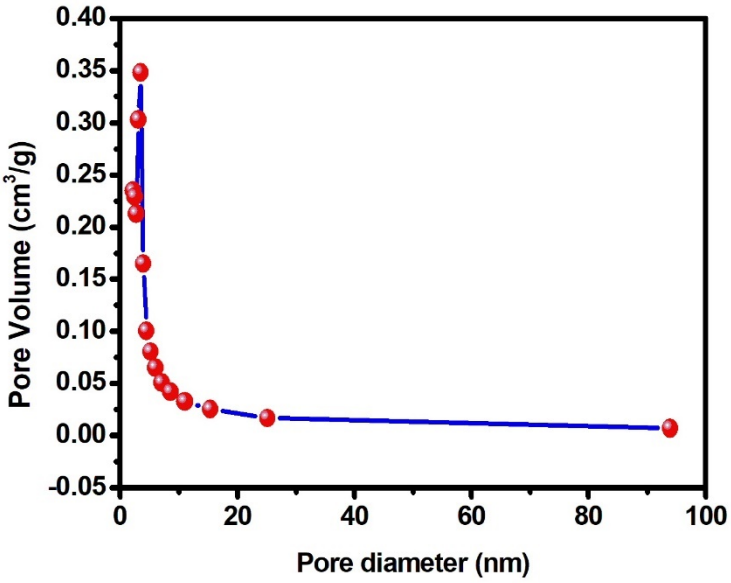

Figure 29 - Pore size distribution of B-Carbon

5.8. Electrochemical Analysis of B-Carbon

5.8.1. Cyclic Voltammetry analysis of B-Carbon

CV analysis of B-Carbon has been carried out in the potential window of -1.0V to - 0.2V. It exhibits the mixed behavior of EDLC and pseudocapacitance and is similar to that of S-Carbon. However, compared to the CV curves of S- carbon, the porous structured B-Carbon exhibits redox peaks which are seen in Figure 30. The oxidation and reduction potentials are clearly observed at the 10mV/s and it gets faded with higher scan rates. The redox potential is -0.25V and it becomes more negative upto -0.37 with increment of scan rate. This is a phenomenon related to electrochemical irreversibility or high barrier to electron transfer making the electron transfer to be sluggish in the electrochemical system. This is possible in the constructed three electrode system in this case with Pt Vs B-Carbon, KOH used is 84% pure with traces of Pb and sulphates. The redox potential of $PbSO_4$ is -0.36V and redox of SO_4 is -0.25.

The specific capacitance values of B-Carbon are 192, 168, 132, 116, 97, and 82 Fg^{-1} at the scan rates of 10, 20, 40, 60, 80, and 100 mV/s respectively. The specific capacitance value has decreased with increase of scan rate. Similar trend has been followed in the case of S-Carbon. However, reversibility of B-Carbon sample is revealed by unchanged CV pattern of the sample even at higher scan rate (100 mV/s).

5.8.2. Galvanostatic Charge-Discharge Analysis of B-Carbon

GCD analysis further confirms the capacitive behavior of B-Carbon. The electrochemical potential window of GCD analysis is from -1.0 to -0.2 V which has been determined from CV analysis. The corresponding GCD curve is given in Figure 31. It indicates that electrochemical performance of the B-Carbon resulted in electric double layer and pseudo capacitive behavior, which is validated by CV data. In GCD analysis of B-Carbon, no significant IR drop is observed which implies that the electrochemical system has low energy dissipation. Also, the longer discharge time has been observed for B-Carbon when compared to S-Carbon. It obviously increases the specific capacitance value according to Eq (2) which is given in Chapter 3. The values of specific capacitance are 198, 176, 135, 105 and 56 Fg^{-1} for current densities of 1, 1.5, 2, 2.5 and 3 Ag^{-1} respectively and well corresponds to the specific capacitance obtained from CV results.

The specific capacitance decreases as the current density increases which is same as that of S- Carbon, shown in Figure 32. Obviously, B-Carbon exhibits the higher specific capacitance (198 Fg^{-1}) than the S- Carbon (84 Fg^{-1}) attributed to high surface area (703 m^2g^{-1}) evidenced by BET analysis and scrambled graphitic mesh like structure as seen in HRTEM micrographs. During GCD analysis, micropores in the B-Carbon serve as ion traps for charge storage, while mesopores provide dual functionalities say, surface for ion adsorption and facilitation of ion transport. In this case, B-Carbon has higher concentration of micropores and considerable amount of mesopores which helps to achieve the higher specific capacitance than S-Carbon.

The specific capacitance of B-Carbon compared with the previously reported work on various biomass are given in Table 10 (previous Chapter 4). Most of the reported results show the lower specific capacitance than the present case. The discussion of preparation and activation methods and non-employment of chemical activation holds good hitherto.

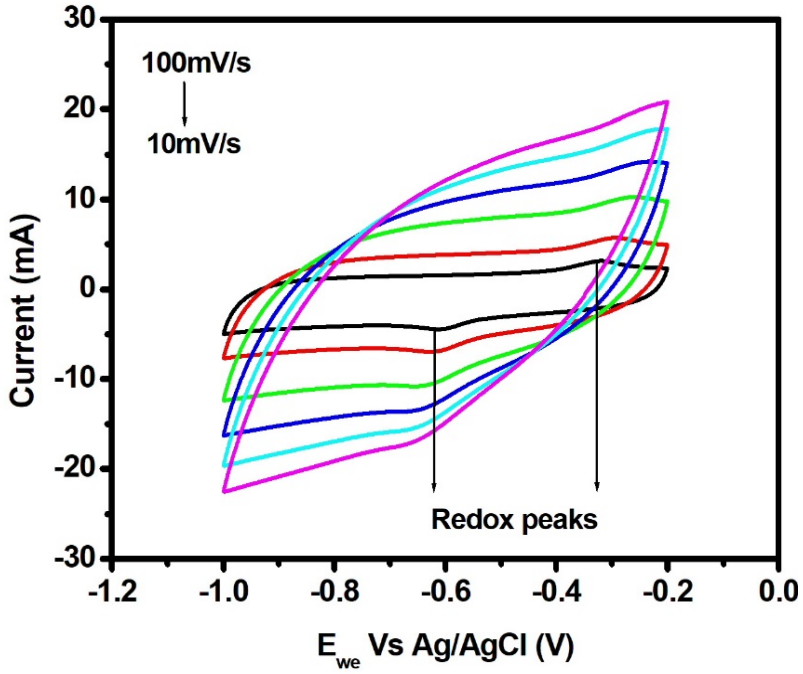

Figure 30 - Cyclic voltammogram of B-Carbon

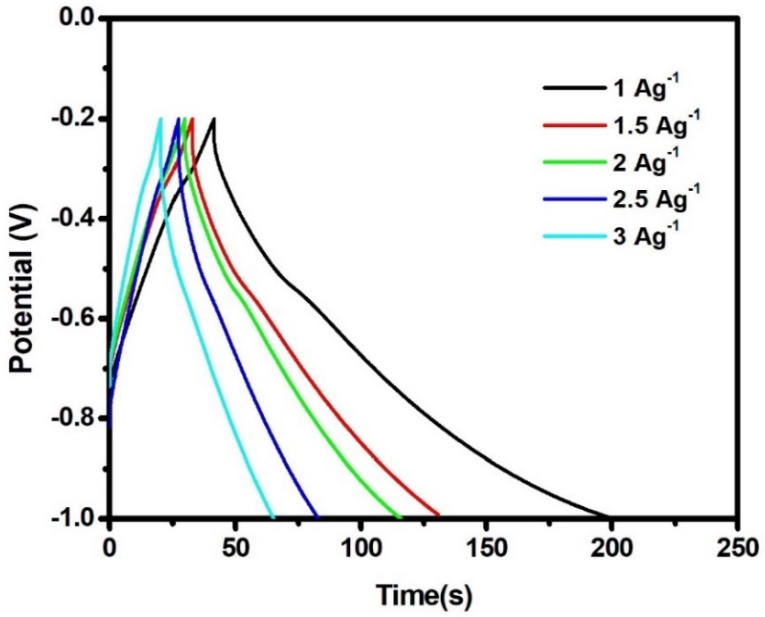

Figure 31 - Galvanostatic Charge-Discharge curves of B-Carbon

In general, the current collector plays an important role to enhance the performance of the material. The usage of Ni foam, in the works reported in the literature, boosts up the

specific capacitance in contrary, in the present study usage of copper current collectors results in reduced specific capacitance. However, the utility of copper collector is advantageous in terms of cost reduction and feasibility for large scale production.

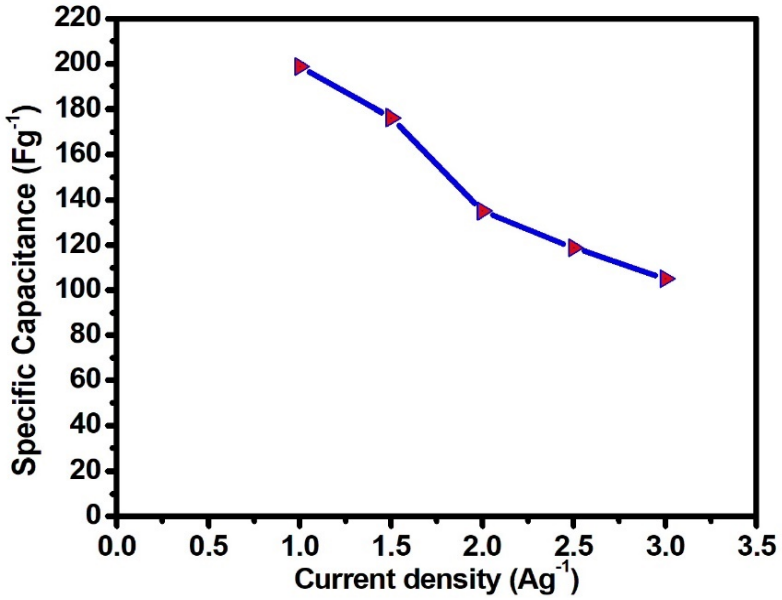

Figure 32 - Plot of current density vs specific capacitance of B-Carbon

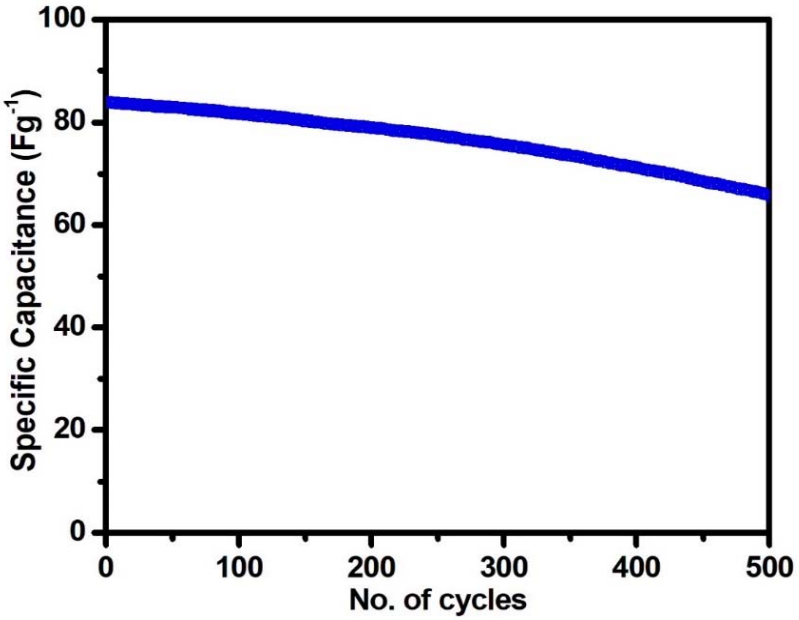

Figure 33 - Cyclic stability of B-Carbon

The cyclic stability of the carbon from the bark *P. juliflora* has been evaluated and shown in Figure 33. The B-Carbon material maintained 77% of its initial specific capacitance for continuous 500 charge/discharge cycles. As discussed in the CV analysis of B Carbon, the stability is reduced due to the impurities which makes the electrochemical redox reaction irreversible thus bringing down the cyclic stability.

5.8.3. Electrochemical Impedance Analysis of B-Carbon

EIS analysis has been carried out in the frequency range from 500 mHz to 10 KHz for B-Carbon. Figure 34 shows the Nyquist plot of B-Carbon. It consists of semicircle in the high frequency region and spike in the low frequency region. Before cycling, the value of solution resistance (R_1) and charge transfer resistance (R_2) are 3.51 Ω and 2.28 Ω respectively. The charge transfer resistance is smaller for B-Carbon when compared to S-Carbon indicating the higher conductivity behaviour of the B-Carbon. However, after cycling, the charge transfer resistance is increased from 2.28 to 16.36 Ω which is due to the formation of irreversible layer and/or SEI layer as discussed in the previous section. As a result of unintentional impurity migration involved in the redox activity results in capacitance fading to 77% after 500 cycles in B-Carbon. The spike at low frequency region of B-Carbon goes more parallel to imaginary axis compared to S-Carbon indicating higher capacitive behaviour of the sample. Further, the Nyquist plot is fitted by an equivalent circuit and is shown in the inset, and the relevant fitted parameters are included in Table 13.

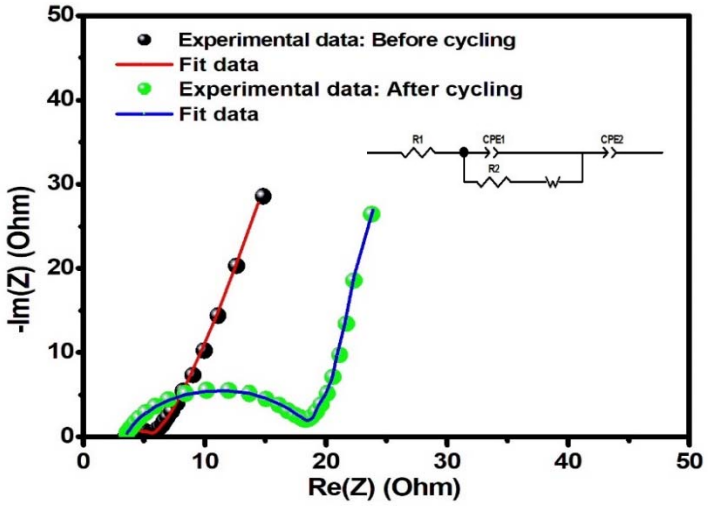

Figure 34 - Electrochemical impedance spectra of B-Carbon before and after cycling

The high electrochemical performance of B-Carbon than S-Carbon has been attributed to the following reasons: (i) Scrambled mesh like highly disordered graphitic structure of the B-carbon seen from the HRTEM analysis (ii) higher atomic weight percentage of carbon observed from EDAX analysis (iii) abundant micropores resulting in high specific surface area value which is obtained from the BET analysis.

Table 13 - Fitted parameters of electrochemical impedance spectra of B-Carbon

Parameters	Before Cycling	After Cycling
$R_1(\Omega)$	3.51	3.75
$R_2(\Omega)$	2.28	16.36
CPE 1	0.67×10^{-3}	0.39×10^{-3}
n1	0.57	0.81
CPE 2	0.09	0.07
n2	0.86	0.99
W	0.20	4.16

5.9. Summary

The carbon prepared from Bark of *Prosopis juliflora* named as B-Carbon by conventional heating after pre-treatment of the biomass yielded higher degree of graphitization compared to S-Carbon discussed in the previous Chapter. The XRD peaks indicated blunt peaks due to disorderliness of graphite and graphitization is confirmed with two planes at (002) and (101). The Raman analysis also vouched the degree of graphitization and also additionally indicated the presence of impurities which alters the band structure of the carbon with D' band at 423 cm^{-1} and influence of D" in 2D+D" at 2900 cm^{-1}. The Morphological micrographs with FESEM and HRTEM confirmed the highly disordered graphitic structures. The BET analysis shows high specific area of 703 m^2g^{-1}. Electrochemical analysis shows cycling stability of 77% over 500 cycles. The fading is attributed to the impurities of electrolyte and not with the working electrode prepared.